FERMILAB-PUB-14-061-E

Mass and lifetime measurements of bottom and charm baryons in $p\bar{p}$ collisions at $\sqrt{s}$ = 1.96 TeV

T. Aaltonen,[21] S. Amerio[jj],[39] D. Amidei,[31] A. Anastassov[v],[15] A. Annovi,[17] J. Antos,[12] G. Apollinari,[15] J.A. Appel,[15] T. Arisawa,[52] A. Artikov,[13] J. Asaadi,[47] W. Ashmanskas,[15] B. Auerbach,[2] A. Aurisano,[47] F. Azfar,[38] W. Badgett,[15] T. Bae,[25] A. Barbaro-Galtieri,[26] V.E. Barnes,[43] B.A. Barnett,[23] P. Barria[ll],[41] P. Bartos,[12] M. Bauce[jj],[39] F. Bedeschi,[41] S. Behari,[15] G. Bellettini[kk],[41] J. Bellinger,[54] D. Benjamin,[14] A. Beretvas,[15] A. Bhatti,[45] K.R. Bland,[5] B. Blumenfeld,[23] A. Bocci,[14] A. Bodek,[44] D. Bortoletto,[43] J. Boudreau,[42] A. Boveia,[11] L. Brigliadori[ii],[6] C. Bromberg,[32] E. Brucken,[21] J. Budagov,[13] H.S. Budd,[44] K. Burkett,[15] G. Busetto[jj],[39] P. Bussey,[19] P. Butti[kk],[41] A. Buzatu,[19] A. Calamba,[10] S. Camarda,[4] M. Campanelli,[28] F. Canelli[cc],[11] B. Carls,[22] D. Carlsmith,[54] R. Carosi,[41] S. Carrillo[l],[16] B. Casal[j],[9] M. Casarsa,[48] A. Castro[ii],[6] P. Catastini,[20] D. Cauz[qqrr],[48] V. Cavaliere,[22] M. Cavalli-Sforza,[4] A. Cerri[e],[26] L. Cerrito[q],[28] Y.C. Chen,[1] M. Chertok,[7] G. Chiarelli,[41] G. Chlachidze,[15] K. Cho,[25] D. Chokheli,[13] A. Clark,[18] C. Clarke,[53] M.E. Convery,[15] J. Conway,[7] M. Corbo[y],[15] M. Cordelli,[17] C.A. Cox,[7] D.J. Cox,[7] M. Cremonesi,[41] D. Cruz,[47] J. Cuevas[x],[9] R. Culbertson,[15] N. d'Ascenzo[u],[15] M. Datta[ff],[15] P. de Barbaro,[44] L. Demortier,[45] M. Deninno,[6] M. D'Errico[jj],[39] F. Devoto,[21] A. Di Canto[kk],[41] B. Di Ruzza[p],[15] J.R. Dittmann,[5] S. Donati[kk],[41] M. D'Onofrio,[27] M. Dorigo[ss],[48] A. Driutti[qqrr],[48] K. Ebina,[52] R. Edgar,[31] A. Elagin,[47] R. Erbacher,[7] S. Errede,[22] B. Esham,[22] S. Farrington,[38] J.P. Fernández Ramos,[29] R. Field,[16] G. Flanagan[s],[15] R. Forrest,[7] M. Franklin,[20] J.C. Freeman,[15] H. Frisch,[11] Y. Funakoshi,[52] C. Galloni[kk],[41] A.F. Garfinkel,[43] P. Garosi[ll],[41] H. Gerberich,[22] E. Gerchtein,[15] S. Giagu,[46] V. Giakoumopoulou,[3] K. Gibson,[42] C.M. Ginsburg,[15] N. Giokaris,[3] P. Giromini,[17] G. Giurgiu,[23] V. Glagolev,[13] D. Glenzinski,[15] M. Gold,[34] D. Goldin,[47] A. Golossanov,[15] G. Gomez,[9] G. Gomez-Ceballos,[30] M. Goncharov,[30] O. González López,[29] I. Gorelov,[34] A.T. Goshaw,[14] K. Goulianos,[45] E. Gramellini,[6] S. Grinstein,[4] C. Grosso-Pilcher,[11] R.C. Group,[51, 15] J. Guimaraes da Costa,[20] S.R. Hahn,[15] J.Y. Han,[44] F. Happacher,[17] K. Hara,[49] M. Hare,[50] R.F. Harr,[53] T. Harrington-Taber[m],[15] K. Hatakeyama,[5] C. Hays,[38] J. Heinrich,[40] M. Herndon,[54] A. Hocker,[15] Z. Hong,[47] W. Hopkins[f],[15] S. Hou,[1] R.E. Hughes,[35] U. Husemann,[55] M. Hussein[aa],[32] J. Huston,[32] G. Introzzi[nnoo],[41] M. Iori[pp],[46] A. Ivanov[o],[7] E. James,[15] D. Jang,[10] B. Jayatilaka,[15] E.J. Jeon,[25] S. Jindariani,[15] M. Jones,[43] K.K. Joo,[25] S.Y. Jun,[10] T.R. Junk,[15] M. Kambeitz,[24] T. Kamon,[25, 47] P.E. Karchin,[53] A. Kasmi,[5] Y. Kato[n],[37] W. Ketchum[gg],[11] J. Keung,[40] B. Kilminster[cc],[15] D.H. Kim,[25] H.S. Kim,[25] J.E. Kim,[25] M.J. Kim,[17] S.H. Kim,[49] S.B. Kim,[25] Y.J. Kim,[25] Y.K. Kim,[11] N. Kimura,[52] M. Kirby,[15] K. Knoepfel,[15] K. Kondo,[52, *] D.J. Kong,[25] J. Konigsberg,[16] A.V. Kotwal,[14] M. Kreps,[24] J. Kroll,[40] M. Kruse,[14] T. Kuhr,[24] M. Kurata,[49] A.T. Laasanen,[43] S. Lammel,[15] M. Lancaster,[28] K. Lannon[w],[35] G. Latino[ll],[41] H.S. Lee,[25] J.S. Lee,[25] S. Leo,[41] S. Leone,[41] J.D. Lewis,[15] A. Limosani[r],[14] E. Lipeles,[40] A. Lister[a],[18] H. Liu,[51] Q. Liu,[43] T. Liu,[15] S. Lockwitz,[55] A. Loginov,[55] D. Lucchesi[jj],[39] A. Lucà,[17] J. Lueck,[24] P. Lujan,[26] P. Lukens,[15] G. Lungu,[45] J. Lys,[26] R. Lysak[d],[12] R. Madrak,[15] P. Maestro[ll],[41] S. Malik,[45] G. Manca[b],[27] A. Manousakis-Katsikakis,[3] L. Marchese[hh],[6] F. Margaroli,[46] P. Marino[mm],[41] M. Martínez,[4] K. Matera,[22] M.E. Mattson,[53] A. Mazzacane,[15] P. Mazzanti,[6] R. McNulty[i],[27] A. Mehta,[27] P. Mehtala,[21] C. Mesropian,[45] T. Miao,[15] D. Mietlicki,[31] A. Mitra,[1] H. Miyake,[49] S. Moed,[15] N. Moggi,[6] C.S. Moon[y],[15] R. Moore[ddee],[15] M.J. Morello[mm],[41] A. Mukherjee,[15] Th. Muller,[24] P. Murat,[15] M. Mussini[ii],[6] J. Nachtman[m],[15] Y. Nagai,[49] J. Naganoma,[52] I. Nakano,[36] A. Napier,[50] J. Nett,[47] C. Neu,[51] T. Nigmanov,[42] L. Nodulman,[2] S.Y. Noh,[25] O. Norniella,[22] L. Oakes,[38] S.H. Oh,[14] Y.D. Oh,[25] I. Oksuzian,[51] T. Okusawa,[37] R. Orava,[21] L. Ortolan,[4] C. Pagliarone,[48] E. Palencia[e],[9] P. Palni,[34] V. Papadimitriou,[15] W. Parker,[54] G. Pauletta[qqrr],[48] M. Paulini,[10] C. Paus,[30] T.J. Phillips,[14] G. Piacentino,[41] E. Pianori,[40] J. Pilot,[7] K. Pitts,[22] C. Plager,[8] L. Pondrom,[54] S. Poprocki[f],[15] K. Potamianos,[26] A. Pranko,[26] F. Prokoshin[z],[13] F. Ptohos[g],[17] G. Punzi[kk],[41] N. Ranjan,[43] I. Redondo Fernández,[29] P. Renton,[38] M. Rescigno,[46] F. Rimondi,[6, *] L. Ristori,[41, 15] A. Robson,[19] T. Rodriguez,[40] S. Rolli[h],[50] M. Ronzani[kk],[41] R. Roser,[15] J.L. Rosner,[11] F. Ruffini[ll],[41] A. Ruiz,[9] J. Russ,[10] V. Rusu,[15] W.K. Sakumoto,[44] Y. Sakurai,[52] L. Santi[qqrr],[48] K. Sato,[49] V. Saveliev[u],[15] A. Savoy-Navarro[y],[15] P. Schlabach,[15] E.E. Schmidt,[15] T. Schwarz,[31] L. Scodellaro,[9] F. Scuri,[41] S. Seidel,[34] Y. Seiya,[37] A. Semenov,[13] F. Sforza[kk],[41] S.Z. Shalhout,[7] T. Shears,[27] P.F. Shepard,[42] M. Shimojima[t],[49] M. Shochet,[11] I. Shreyber-Tecker,[33] A. Simonenko,[13] K. Sliwa,[50] J.R. Smith,[7] F.D. Snider,[15] H. Song,[42] V. Sorin,[4] R. St. Denis,[19, *] M. Stancari,[15] D. Stentz[v],[15] J. Strologas,[34] Y. Sudo,[49] A. Sukhanov,[15] I. Suslov,[13] K. Takemasa,[49] Y. Takeuchi,[49] J. Tang,[11] M. Tecchio,[31] P.K. Teng,[1] J. Thom[f],[15] E. Thomson,[40] V. Thukral,[47] D. Toback,[47] S. Tokar,[12] K. Tollefson,[32] T. Tomura,[49] D. Tonelli[e],[15] S. Torre,[17] D. Torretta,[15] P. Totaro,[39] M. Trovato[mm],[41] F. Ukegawa,[49] S. Uozumi,[25] F. Vázquez[l],[16] G. Velev,[15] C. Vellidis,[15] C. Vernieri[mm],[41] M. Vidal,[43] R. Vilar,[9] J. Vizán[bb],[9] M. Vogel,[34] G. Volpi,[17] P. Wagner,[40] R. Wallny[j],[15] S.M. Wang,[1] D. Waters,[28]

Operated by Fermi Research Alliance, LLC under Contract No. De-AC02-07CH11359 with the United States Department of Energy.

W.C. Wester III,[15] D. Whiteson[c],[40] A.B. Wicklund,[2] S. Wilbur,[7] H.H. Williams,[40] J.S. Wilson,[31] P. Wilson,[15] B.L. Winer,[35] P. Wittich[f],[15] S. Wolbers,[15] H. Wolfe,[35] T. Wright,[31] X. Wu,[18] Z. Wu,[5] K. Yamamoto,[37] D. Yamato,[37] T. Yang,[15] U.K. Yang,[25] Y.C. Yang,[25] W.-M. Yao,[26] G.P. Yeh,[15] K. Yi[m],[15] J. Yoh,[15] K. Yorita,[52] T. Yoshida[k],[37] G.B. Yu,[14] I. Yu,[25] A.M. Zanetti,[48] Y. Zeng,[14] C. Zhou,[14] and S. Zucchelli[ii]6

(CDF Collaboration)[, †]

[1]*Institute of Physics, Academia Sinica, Taipei, Taiwan 11529, Republic of China*
[2]*Argonne National Laboratory, Argonne, Illinois 60439, USA*
[3]*University of Athens, 157 71 Athens, Greece*
[4]*Institut de Fisica d'Altes Energies, ICREA, Universitat Autonoma de Barcelona, E-08193, Bellaterra (Barcelona), Spain*
[5]*Baylor University, Waco, Texas 76798, USA*
[6]*Istituto Nazionale di Fisica Nucleare Bologna,* [ii]*University of Bologna, I-40127 Bologna, Italy*
[7]*University of California, Davis, Davis, California 95616, USA*
[8]*University of California, Los Angeles, Los Angeles, California 90024, USA*
[9]*Instituto de Fisica de Cantabria, CSIC-University of Cantabria, 39005 Santander, Spain*
[10]*Carnegie Mellon University, Pittsburgh, Pennsylvania 15213, USA*
[11]*Enrico Fermi Institute, University of Chicago, Chicago, Illinois 60637, USA*
[12]*Comenius University, 842 48 Bratislava, Slovakia; Institute of Experimental Physics, 040 01 Kosice, Slovakia*
[13]*Joint Institute for Nuclear Research, RU-141980 Dubna, Russia*
[14]*Duke University, Durham, North Carolina 27708, USA*
[15]*Fermi National Accelerator Laboratory, Batavia, Illinois 60510, USA*
[16]*University of Florida, Gainesville, Florida 32611, USA*
[17]*Laboratori Nazionali di Frascati, Istituto Nazionale di Fisica Nucleare, I-00044 Frascati, Italy*
[18]*University of Geneva, CH-1211 Geneva 4, Switzerland*
[19]*Glasgow University, Glasgow G12 8QQ, United Kingdom*
[20]*Harvard University, Cambridge, Massachusetts 02138, USA*
[21]*Division of High Energy Physics, Department of Physics, University of Helsinki, FIN-00014, Helsinki, Finland; Helsinki Institute of Physics, FIN-00014, Helsinki, Finland*
[22]*University of Illinois, Urbana, Illinois 61801, USA*
[23]*The Johns Hopkins University, Baltimore, Maryland 21218, USA*
[24]*Institut für Experimentelle Kernphysik, Karlsruhe Institute of Technology, D-76131 Karlsruhe, Germany*
[25]*Center for High Energy Physics: Kyungpook National University, Daegu 702-701, Korea; Seoul National University, Seoul 151-742, Korea; Sungkyunkwan University, Suwon 440-746, Korea; Korea Institute of Science and Technology Information, Daejeon 305-806, Korea; Chonnam National University, Gwangju 500-757, Korea; Chonbuk National University, Jeonju 561-756, Korea; Ewha Womans University, Seoul, 120-750, Korea*
[26]*Ernest Orlando Lawrence Berkeley National Laboratory, Berkeley, California 94720, USA*
[27]*University of Liverpool, Liverpool L69 7ZE, United Kingdom*
[28]*University College London, London WC1E 6BT, United Kingdom*
[29]*Centro de Investigaciones Energeticas Medioambientales y Tecnologicas, E-28040 Madrid, Spain*
[30]*Massachusetts Institute of Technology, Cambridge, Massachusetts 02139, USA*
[31]*University of Michigan, Ann Arbor, Michigan 48109, USA*
[32]*Michigan State University, East Lansing, Michigan 48824, USA*
[33]*Institution for Theoretical and Experimental Physics, ITEP, Moscow 117259, Russia*
[34]*University of New Mexico, Albuquerque, New Mexico 87131, USA*
[35]*The Ohio State University, Columbus, Ohio 43210, USA*
[36]*Okayama University, Okayama 700-8530, Japan*
[37]*Osaka City University, Osaka 558-8585, Japan*
[38]*University of Oxford, Oxford OX1 3RH, United Kingdom*
[39]*Istituto Nazionale di Fisica Nucleare, Sezione di Padova,* [jj]*University of Padova, I-35131 Padova, Italy*
[40]*University of Pennsylvania, Philadelphia, Pennsylvania 19104, USA*
[41]*Istituto Nazionale di Fisica Nucleare Pisa,* [kk]*University of Pisa,* [ll]*University of Siena,* [mm]*Scuola Normale Superiore, I-56127 Pisa, Italy,* [nn]*INFN Pavia, I-27100 Pavia, Italy,* [oo]*University of Pavia, I-27100 Pavia, Italy*
[42]*University of Pittsburgh, Pittsburgh, Pennsylvania 15260, USA*
[43]*Purdue University, West Lafayette, Indiana 47907, USA*
[44]*University of Rochester, Rochester, New York 14627, USA*
[45]*The Rockefeller University, New York, New York 10065, USA*
[46]*Istituto Nazionale di Fisica Nucleare, Sezione di Roma 1,* [pp]*Sapienza Università di Roma, I-00185 Roma, Italy*

[47]Mitchell Institute for Fundamental Physics and Astronomy, Texas A&M University, College Station, Texas 77843, USA
[48]Istituto Nazionale di Fisica Nucleare Trieste, [qq]Gruppo Collegato di Udine, [rr]University of Udine, I-33100 Udine, Italy, [ss]University of Trieste, I-34127 Trieste, Italy
[49]University of Tsukuba, Tsukuba, Ibaraki 305, Japan
[50]Tufts University, Medford, Massachusetts 02155, USA
[51]University of Virginia, Charlottesville, Virginia 22906, USA
[52]Waseda University, Tokyo 169, Japan
[53]Wayne State University, Detroit, Michigan 48201, USA
[54]University of Wisconsin, Madison, Wisconsin 53706, USA
[55]Yale University, New Haven, Connecticut 06520, USA

We report on mass and lifetime measurements of several ground state charmed and bottom baryons, using a data sample corresponding to 9.6 fb^{-1} from $p\bar{p}$ collisions at $\sqrt{s} = 1.96$ TeV, and recorded with the Collider Detector at Fermilab. Baryon candidates are reconstructed from data collected with an online event selection designed for the collection of long-lifetime heavy-flavor decay products and a second event selection designed to collect $J/\psi \to \mu^+\mu^-$ candidates. First evidence for the process $\Omega_b^- \to \Omega_c^0 \pi^-$ is presented with a significance of 3.3σ. We measure the following baryon masses:

$$M(\Xi_c^0) = 2470.85 \pm 0.24(\text{stat}) \pm 0.55(\text{syst})\,\text{MeV}/c^2,$$
$$M(\Xi_c^+) = 2468.00 \pm 0.18(\text{stat}) \pm 0.51(\text{syst})\,\text{MeV}/c^2,$$
$$M(\Lambda_b) = 5620.15 \pm 0.31(\text{stat}) \pm 0.47(\text{syst})\,\text{MeV}/c^2,$$
$$M(\Xi_b^-) = 5793.4 \pm 1.8(\text{stat}) \pm 0.7(\text{syst})\,\text{MeV}/c^2,$$
$$M(\Xi_b^0) = 5788.7 \pm 4.3(\text{stat}) \pm 1.4(\text{syst})\,\text{MeV}/c^2, \text{ and}$$
$$M(\Omega_b^-) = 6047.5 \pm 3.8(\text{stat}) \pm 0.6(\text{syst})\,\text{MeV}/c^2.$$

The isospin splitting of the $\Xi_b^{-,0}$ states is found to be $M(\Xi_b^-) - M(\Xi_b^0) = 4.7 \pm 4.7(\text{stat}) \pm 0.7(\text{syst})$ MeV/c^2. The isospin splitting of the $\Xi_c^{0,+}$ states is found to be $M(\Xi_c^0) - M(\Xi_c^+) = 2.85 \pm 0.30(\text{stat}) \pm 0.04(\text{syst})$ MeV/c^2. The following lifetime measurements are made:

$$\tau(\Lambda_b) = 1.565 \pm 0.035(\text{stat}) \pm 0.020(\text{syst})\,\text{ps},$$
$$\tau(\Xi_b^-) = 1.32 \pm 0.14(\text{stat}) \pm 0.02(\text{syst})\,\text{ps},$$
$$\tau(\Omega_b^-) = 1.66^{+0.53}_{-0.40}(\text{stat}) \pm 0.02(\text{syst})\,\text{ps}.$$

PACS numbers: 13.30.Eg, 13.60.Rj, 14.20.Mr

I. INTRODUCTION

The quark model describes the spectroscopy of hadrons with great success. In particular, this has been the case for the D and B mesons, where all of the ground states have been observed [1]. The spectroscopy of c baryons also agrees well with the quark model, and a rich spectrum of baryons containing b quarks is predicted [2, 3]. The accumulation of large data sets from the Tevatron and Large Hadron Collider has made possible the observation and measurements of most of the b-baryon ground

*Deceased
†With visitors from [a]University of British Columbia, Vancouver, BC V6T 1Z1, Canada, [b]Istituto Nazionale di Fisica Nucleare, Sezione di Cagliari, 09042 Monserrato (Cagliari), Italy, [c]University of California Irvine, Irvine, CA 92697, USA, [d]Institute of Physics, Academy of Sciences of the Czech Republic, 182 21, Czech Republic, [e]CERN, CH-1211 Geneva, Switzerland, [f]Cornell University, Ithaca, NY 14853, USA, [g]University of Cyprus, Nicosia CY-1678, Cyprus, [h]Office of Science, U.S. Department of Energy, Washington, DC 20585, USA, [i]University College Dublin, Dublin 4, Ireland, [j]ETH, 8092 Zürich, Switzerland, [k]University of Fukui, Fukui City, Fukui Prefecture, Japan 910-0017, [l]Universidad Iberoamericana, Lomas de Santa Fe, México, C.P. 01219, Distrito Federal, [m]University of Iowa, Iowa City, IA 52242, USA, [n]Kinki University, Higashi-Osaka City, Japan 577-8502, [o]Kansas State University, Manhattan, KS 66506, USA, [p]Brookhaven National Laboratory, Upton, NY 11973, USA, [q]Queen Mary, University of London, London, E1 4NS, United Kingdom, [r]University of Melbourne, Victoria 3010, Australia, [s]Muons, Inc., Batavia, IL 60510, USA, [t]Nagasaki Institute of Applied Science, Nagasaki 851-0193, Japan, [u]National Research Nuclear University, Moscow 115409, Russia, [v]Northwestern University, Evanston, IL 60208, USA, [w]University of Notre Dame, Notre Dame, IN 46556, USA, [x]Universidad de Oviedo, E-33007 Oviedo, Spain, [y]CNRS-IN2P3, Paris, F-75205 France, [z]Universidad Tecnica Federico Santa Maria, 110v Valparaiso, Chile, [aa]The University of Jordan, Amman 11942, Jordan, [bb]Universite catholique de Louvain, 1348 Louvain-La-Neuve, Belgium, [cc]University of Zürich, 8006 Zürich, Switzerland, [dd]Massachusetts General Hospital, Boston, MA 02114 USA, [ee]Harvard Medical School, Boston, MA 02114 USA, [ff]Hampton University, Hampton, VA 23668, USA, [gg]Los Alamos National Laboratory, Los Alamos, NM 87544, USA, [hh]Università degli Studi di Napoli Federico I, I-80138 Napoli, Italy

states containing a single heavy quark [4–10] and several resonant states [6, 11–13]. The samples of most b baryons accumulated to date are small, and the measurements of the properties of these particles are limited by the sample size. The exception to this is the Λ_b baryon, where the reconstructed samples are now large enough to probe its properties with precision. Early measurements of the Λ_b lifetime disagreed with predictions from heavy-quark expansion theory, if compared with the B^0 lifetime [14]. With the large samples that are now available, precision measurements of the Λ_b lifetime are providing a strong test of the heavy-quark expansion in describing b hadrons [15].

In this paper, we report the measurements of mass and lifetime, τ, for the Λ_b, Ξ_b^- and Ω_b^- baryons through the decay processes $\Lambda_b \to J/\psi\,\Lambda$, $\Xi_b^- \to J/\psi\,\Xi^-$, and $\Omega_b^- \to J/\psi\,\Omega^-$. Mass measurements of the Ξ_c^0, Ξ_c^+, Ξ_b^-, and Ξ_b^0 are made by reconstructing the processes $\Xi_c^0 \to \Xi^-\,\pi^+$, $\Xi_c^+ \to \Xi^-\,\pi^+\,\pi^+$, $\Xi_b^- \to \Xi_c^0\,\pi^-$, and $\Xi_b^0 \to \Xi_c^+\,\pi^-$. In addition, we report first evidence for the process $\Omega_b^- \to \Omega_c^0\,\pi^-$, $\Omega_c^0 \to \Omega^-\,\pi^+$. These decay chains are reconstructed using the processes $J/\psi \to \mu^+\,\mu^-$, $\Xi^- \to \Lambda\,\pi^-$, $\Omega^- \to \Lambda\,K^-$, and $\Lambda \to p\,\pi^-$. Charge conjugate modes are implicitly included. These measurements are made in $p\overline{p}$ collisions at a center-of-mass energy of 1.96 TeV using the Collider Detector at Fermilab (CDF II), corresponding to an integrated luminosity of 9.6 fb^{-1}. This paper uses the full CDF II data set collected during the 2001-11 operation of the Tevatron.

The strategy of this analysis is to calibrate and check the measurement technique on the better known b-meson states and then to extend the method to property measurements of the b baryons reconstructed from the same data. All mass and lifetime measurements are performed on the $B^+ \to J/\psi\,K^+$ and $B^0 \to J/\psi\,K^*(892)^0$, $K^*(892)^0 \to K^+\pi^-$ final states to provide a large sample for comparison to the world-average values. The decay mode $B^0 \to J/\psi\,K_S^0$, $K_S^0 \to \pi^+\,\pi^-$ is also used as a reference process. Although its sample size is smaller than the samples of B^+ and other B^0 decays, this is an appropriate reference because the K_S^0 is reconstructed from charged particles that are significantly displaced from the collision, similar to the final-state particles from the b-baryon decays studied in this work.

We begin with a brief description of the detector and its simulation in Sec. II. In Sec. III, the reconstruction of J/ψ mesons, neutral K mesons, hyperons, and b hadrons is described. In Sec. IV, we present measurements of the properties of the $\Xi_c^{0,+}$, Λ_b, $\Xi_b^{-,0}$, and Ω_b^- baryons, which include particle masses and lifetimes. We conclude in Sec. VI with a summary of the results.

II. DETECTOR DESCRIPTION AND SIMULATION

The CDF II detector has been described in detail elsewhere [16]. This analysis primarily relies upon the charged-particle tracking and muon-identification systems. The tracking system consists of four different detector subsystems that operate inside a 1.4 T solenoid with its axis parallel to the beamline. The first of these is a single layer of silicon strip detectors (L00) at a radius of $1.35 - 1.6$ cm from the axis of the solenoid. It measures charged-particle positions (hits) in the transverse view with respect to the beam, which is parallel to the z direction. A five-layer silicon detector (SVX II). surrounding L00 measures hits at radii of 2.5 to 10.6 cm [17]. Each of these layers provides a transverse measurement and a stereo measurement of 90° (three layers) or ±1.2° (two layers) with respect to the beam direction. The outermost silicon detector lies between 19 cm and 30 cm radially, and provides one or two hits, depending on the track pseudorapidity (η), where $\eta \equiv -\ln[\tan(\theta/2)]$, with θ being the angle between the particle momentum and the proton-beam direction. An open-cell drift chamber (COT) completes the tracking system, and covers the radial region from 43 cm to 132 cm [18]. The COT consists of 96 sense-wire layers, arranged in 8 superlayers of 12 wires each. Four of these superlayers provide axial measurements and four provide stereo views of ±2°. Transverse momentum, p_T, (defined as the component of the particle momentum perpendicular to the proton-beam direction) of charged particles is measured in the COT with a resolution of $\sigma(p_T)/p_T^2 = 0.0017\ [\mathrm{GeV}/c]^{-1}$.

Electromagnetic and hadronic calorimeters surround the solenoid coil. Muon candidates from the decay $J/\psi \to \mu^+\mu^-$ are identified by two sets of drift chambers located radially outside the calorimeters. The central muon chambers cover the region $|\eta| < 0.6$, and detect muons with $p_T > 1.4$ GeV/c [19]. A second muon system covers the region $0.6 < |\eta| < 1.0$ and detects muons with $p_T > 2.0$ GeV/c. Muon selection is based on matching the measurements from these chambers to COT tracks, both in projected position and angle.

The analysis presented here is based on events recorded with two different online event-selection (trigger) algorithms. The first is dedicated to the collection of a $J/\psi \to \mu^+\mu^-$ sample. The first level of the three-level trigger system requires two muon candidates with matching tracks in the COT and muon chambers. The second level imposes the requirement that muon candidates have opposite electric charge and limits the accepted range of azimuthal opening angle. The highest level of the J/ψ trigger reconstructs the muon pair in software, and requires the invariant mass of the pair to fall within the range $2.7 - 4.0$ GeV/c^2.

The second data set used is triggered by a system designed to collect particle candidates that decay with lifetimes characteristic of heavy flavor hadrons. The first level of this trigger requires two charged particles in the COT with $p_T > 2.0$ GeV/c. In the second level of the trigger, the silicon vertex trigger [20] is used to associate SVX II data with the tracks found in the COT to precisely measure the impact parameter (defined as the distance of closest approach in the transverse view) with

respect to the beamline. The impact parameter resolution (typically 40 μm) for these tracks allows the isolation of a track sample that does not originate directly from the $p\bar{p}$ collision [17]. The silicon vertex trigger requires two tracks with impact parameters d in the range $0.1 - 1.0$ mm with respect to the beam and a point of intersection at least 200 μm from the beamline in the transverse view. These and other requirements bias the trigger efficiency toward candidates that have a long decay time. Lifetime measurements made with these data therefore require a careful study of these biases and appropriate corrections. The additional statistical power from lifetime measurements that use these data is insufficient to overcome the systematic uncertainty due to the trigger conditions. Therefore, only mass measurements are extracted from the hadronic trigger data in this work.

The mass resolution and acceptance for the b hadrons used in this analysis are studied with a Monte Carlo simulation that generates b hadrons consistent with CDF measurements of p_T and rapidity distributions. The final-state decay processes are simulated with the EvtGen [21] program, and all simulated b hadrons are produced without polarization. The generated events are input to the detector and trigger simulation based on a GEANT3 description [22] and processed through the same reconstruction and analysis algorithms that are used for the data.

III. PARTICLE RECONSTRUCTION METHODS

A. J/ψ reconstruction

The analysis of the data obtained with the muon trigger begins with a selection of well-measured $J/\psi \to \mu^+\mu^-$ candidates. The trigger requirements are confirmed by selecting events that contain two oppositely charged muon candidates, each with matching COT and muon-chamber tracks. Both muon tracks are required to have associated position measurements in at least three layers of the SVX II. This data sample provides approximately 6.5×10^7 J/ψ candidates, measured with an average mass resolution of approximately 20 MeV/c^2. These candidates are required to have a two-track invariant mass within the range listed in Table I.

B. Neutral Hadron Reconstruction

The reconstruction of K^0_S, $K^*(892)^0$, and Λ candidates uses all particles with $p_T > 0.4$ GeV/c found in the COT that are not associated with muons used in the J/ψ reconstruction or tracks used by the hadronic trigger. Pairs of oppositely charged particles are combined to identify these neutral decay candidates. Silicon detector information is not used on these to avoid decay-length-dependent biases on the reconstruction efficiency due to the long lifetimes of the particles. Candidate selection for these neutral states is based upon the mass calculated for each track pair, which is required to fall within the ranges given in Table I after the appropriate mass assignment is made for each track. Backgrounds to the K^0_S ($c\tau \approx 2.7$ cm) and Λ ($c\tau \approx 7.9$ cm) signals [1] are reduced by imposing requirements on the transverse flight-distance, given for neutral particles as $f(h) \equiv (\vec{r}_d - \vec{r}_o) \cdot \vec{p}_T(h)/|\vec{p}_T(h)|$, where $\vec{p}_T(h)$ is the transverse momentum of the hadron candidate, and $\vec{r}_d, \vec{r}_o$ are the transverse positions of the decay point and point of origin, respectively. The transverse flight-distance of the K^0_S and Λ candidates with respect to the primary vertex (defined as the beam position in the transverse view) is required to be greater than 1.0 cm.

TABLE I: Mass ranges around the known mass values [1] used for the b-hadron decay products.

Resonance (final state)	Mass range (MeV/c^2)
$J/\psi\,(\mu^+\mu^-)$	± 80
$K^*(892)^0\,(K^+\pi^-)$	± 30
$K^0_S\,(\pi^+\pi^-)$	± 20
$\Lambda\,(p\pi^-)$	± 9
$\Xi^-\,(\Lambda\pi^-)$	± 9
$\Omega^-\,(\Lambda K^-)$	± 8
$\Xi^0_c\,(\Xi^-\pi^+)$	± 30
$\Xi^+_c\,(\Xi^-\pi^+\pi^+)$	± 25
$\Omega^0_c\,(\Omega^-\pi^+)$	± 30

C. Charged Hyperon Reconstruction

For events that contain a Λ candidate, the remaining particles reconstructed in the COT, again without additional silicon information, are assigned the pion or kaon mass, and $\Lambda\,\pi^-$ or $\Lambda\,K^-$ combinations are identified that are consistent with the decay process $\Xi^- \to \Lambda\,\pi^-$ or $\Omega^- \to \Lambda\,K^-$. Candidates are required to have a mass that is consistent with the ranges listed in Table I. Charged particles with p_T as low as 0.4 GeV/c are used for Ξ^- reconstruction. However, event simulation indicates that the p_T distribution of K^- mesons produced from Ω^- decays has a higher average value, and declines more slowly, than the p_T distribution of the pions from Λ or Ξ^- decays. Therefore, $p_T(K^-) > 1.0$ GeV/c is required for the Ω^- sample.

Several features of the track topology are used to reduce the Ξ^- and Ω^- backgrounds. In order to improve the mass resolution for Ξ^- and Ω^- candidates, the reconstruction requires a good fit of the three tracks that simultaneously constrains the Λ decay products to the Λ mass, and the Λ trajectory to intersect with the helix of the $\pi^-(K^-)$ originating from the $\Xi^-(\Omega^-)$ candidate. In addition, the transverse flight-distance of the Λ candidate with respect to the reconstructed decay vertex of

the $\Xi^-(\Omega^-)$ candidate is required to exceed 1.0 cm. Due to the long lifetime of the Ξ^- ($c\tau \approx 4.9$ cm) and Ω^- ($c\tau \approx 2.5$ cm) particles [1], a transverse flight-distance of at least 1.0 cm (corresponding to a measurement uncertainty of approximately one standard deviation for a typical candidate) with respect to the primary vertex is required. Transverse flight-distance for charged particles is defined as the arc length from the point of closest approach to the origin to the decay point. Possible kinematic reflections are removed from the Ω^- sample by requiring that the combinations in the sample fall outside the Ξ^- mass range listed in Table I when the candidate K^- track is assigned the mass of the π^-. In instances where the correct vertex assignment for the decay tracks is ambiguous, a fit is performed for all configurations and a single, preferred candidate is chosen by retaining only the fit combination with the lowest χ^2.

D. Charmed Hyperon Reconstruction

The Ξ^- and Ω^- candidates are used to reconstruct the processes $\Xi_c^0 \to \Xi^-\,\pi^+$, $\Xi_c^+ \to \Xi^-\,\pi^+\,\pi^+$, and $\Omega_c^0 \to \Omega^-\,\pi^+$. Each c-baryon candidate is subjected to a simultaneous fit of all the tracks in the decay process that constrains the track intersections and decay product momenta to be consistent with the appropriate decay topology. In addition, the tracks from the Λ decay are constrained to the known Λ mass.

The kinematic properties of Ξ^- and Ω^- decays and the lower p_T limit of 0.4 GeV/c on the final-state tracks cause the majority of accepted charged hyperon candidates to have $p_T > 1.5$ GeV/c. This fact, along with the long lifetimes of the Ξ^- and Ω^-, results in a significant fraction of hyperon candidates having decay vertices located several centimeters radially outward from the beam position. Therefore, we refine the charged-hyperon reconstruction by using the improved determination of its trajectory available from tracking these particles in the silicon detector. The $\Xi^-(\Omega^-)$ point of origin, point of decay, and momentum obtained from the full four- or five-track fit are used to define a helix that serves as the seed for an algorithm that associates silicon detector hits with the charged-hyperon track. Charged-hyperon candidates with track measurements in at least one layer of the silicon detector have excellent impact parameter resolution (average of 60 μm) for the charged hyperon track.

Mass distributions are shown in Fig. 1 for all combinations and for the subset where the Ξ^- or Ω^- track reconstruction is improved by using at least one hit in the SVX II and the impact parameter of the c baryon with respect to the beam is less than 100 μm. The improvement in charmed-hyperon purity is evident. An estimate of the yield in each case is made by performing a binned fit on these distributions, which models the data with a Gaussian signal and linear background. Due to the small sample size, the Gaussian width term for the Ω_c^0 is fixed at 8 MeV/c^2, which is the resolution predicted by the event simulation. The background under each signal is estimated by integrating the background function from the fit over the range $\pm 2\sigma$ around the signal mass, where σ is the characteristic width of the Gaussian signal. Signal yields and purity, defined as signal-to-background ratio, are listed in Table II for all fits. A requirement of

TABLE II: Signal yields and purity for charmed hyperon samples. Only statistical uncertainties are listed.

State	Full sample		Tracked in SVX II	
	Yield	Purity	Yield	Purity
Ξ_c^0	5614 ± 247	0.15 ± 0.01	3412 ± 84	0.63 ± 0.01
Ξ_c^+	7984 ± 354	0.11 ± 0.01	5065 ± 104	0.61 ± 0.01
Ω_c^0	416 ± 135	0.03 ± 0.01	124 ± 31	0.22 ± 0.05

silicon-detector information on the Ξ^- candidate track is approximately 60% efficient for the inclusive Ξ_c baryon sample. Signal purity increases markedly when the silicon is used. The efficiency of this requirement on the Ω^- signal is lower, as expected from the shorter lifetime of the Ω^-. A substantial fraction of Ω^- decay prior to reaching the SVX II, so they fall outside the acceptance of the detector. However, the use of silicon when it is available provides a significant improvement in signal purity. Consequently, charmed hyperon candidates retained for further analysis are required to have a Ξ^- or Ω^- candidate measured in the silicon detector. At least one π^+ with $p_T > 2.0$ GeV/c and $d > 100\,\mu$m is required, for consistency with the trigger. We also require $p_T > 4.0$ GeV/c and $ct > 100\,\mu$m for the charmed hyperon candidates, where t is the measured decay time given by $t = f\,M/p_T$, M is the reconstructed mass of the candidate, and f is the transverse flight distance defined in Sec. III B.

E. b baryon reconstruction

A good fit is required on the final-state tracks of all b-baryon candidates that constrains them to originate from the vertices appropriate for the particular decay channel being considered. In addition, we require $ct > 100\,\mu$m and $d < 100\,\mu$m for each b-baryon candidate, to remove prompt and poorly reconstructed candidates. All hadron decay products used in the b-baryon reconstruction are required to have a measured mass consistent with the known values, according to the ranges listed in Table I.

Several selection criteria are used that are common to all b-hadron candidates with a J/ψ meson in the final state. We require the transverse momentum of the b hadron to exceed 6.0 GeV/c and $p_T(h) > 2.0$ GeV/c, where h is the hadron accompanying the J/ψ meson. These requirements reduce combinatorial background. In addition, the final-state fit constrains the mass of the $\mu^+\,\mu^-$ pair to the known mass of the J/ψ meson [1]. The

hadron tracks are reconstructed without silicon-detector information. Therefore, all b-hadron decay position information is derived solely from the muons, and the decay-time resolution is simular for all b hadrons in this data set.

The hadronic trigger data provides a sample of Ξ_b baryons through the decay channel $\Xi_b \to \Xi_c\,\pi^-$, $\Xi_c \to \Xi^-\,\pi^+\,(\pi^+)$, $\Xi^- \to \Lambda\,\pi^-$, and $\Lambda \to p\,\pi^-$. A similar decay chain is used for Ω_b^- reconstruction. The final-state track fit used in these decay processes includes a constraint on the Λ decay products to the known Λ mass. The π^- candidates from the b-baryon decay are required to have electric charge opposite to the Λ baryon number, and to be consistent with having satisfied the trigger by having $p_T > 2.0$ GeV/c and $d > 100\,\mu$m. The backgrounds under the Ξ_b states are also reduced by restricting the sample based on the measured decay time of the Ξ_c candidates to the range $-2\sigma_t < t(\Xi_c) < 3\tau_0(\Xi_c) + 2\sigma_t$, where σ_t is the calculated uncertainty on the decay time and $\tau_0(\Xi_c)$ is the known lifetime of the appropriate Ξ_c baryon [1].

The lifetime of the Ω_c^0 is so short ($c\tau \approx 21\,\mu$m) [1] that the tracking system has no ability to resolve it. Consequently, no $t(\Omega_c^0)$ requirement is made in the selection of $\Omega_c^0\,\pi^-$ combinations. Figure 2 shows $\Omega^-\,\pi^+$ and $\Omega^-\,\pi^+\,\pi^-$ mass distributions of selected combinations. Figure 2(a) shows the distribution of all $\Omega^-\,\pi^+$ combinations that, combined with a π^- candidate, yield a mass within 50 MeV/c^2 of the Ω_b^- mass previously measured by this experiment [8]. The known mass of the Ω_c^0 [1] is also indicated. The $\Omega^-\,\pi^+$ combinations shown in Fig. 2(b) are chosen from two $\Omega^-\,\pi^+\,\pi^-$ mass sidebands, selected to be 50 MeV/c^2 in width and centered at $\pm$100 MeV/c^2 from the Ω_b^- mass. There is a clear indication of Ω_c^0 candidates in events where the $\Omega^-\,\pi^+\,\pi^-$ mass is consistent with the Ω_b^- mass, whereas no enhancement compatible with an Ω_c^0 signal appears in the background sample. A similar comparison is made between Figs. 2(c) and 2(d), where the $\Omega^-\,\pi^+\,\pi^-$ mass is shown for candidates consistent with Ω_c^0 decays and candidates from the sidebands of the $\Omega^-\,\pi^+$ mass distribution.

F. Evidence for the $\Omega_b^- \to \Omega_c^0\,\pi^-$ decay

The indication of an Ω_b^- signal in the $\Omega_c^0\,\pi^-$ mass distribution shown in Fig. 2(c) requires additional consideration. Because the process $\Omega_b^- \to \Omega_c^0\,\pi^-$ has never been observed, a standard significance test is performed where the mass distribution is fit once with a signal amplitude that is allowed to float and once where it is fixed to zero (the null hypothesis). The signal mass used is fixed and the measurement resolution is fixed to 20 MeV/c^2, as determined by the simulation. Two different Ω_b^- mass assumptions are used, corresponding to the value measured in this work, and the value recently measured by the LHCb Collaboration [10], in order to assess the sensitivity of the significance to the mass value. Twice the change in the logarithm of the fit likelihood between the null and floating signal hypotheses, $2\Delta\ln\mathcal{L}$, is found to be 10.3 and 13.3 for the different Ω_b^- mass assumptions.

The probability that the signal shown in Fig. 2(c) arises from a background fluctuation is obtained from a simple simulation of the distribution of ten independent mass values generated uniformly over the range used in Fig. 2(c). The generated unbinned distribution is then fit with the likelihood function twice, as is done with the data. The value of $2\Delta\ln\mathcal{L}$ between the two fits is then recorded. The process is repeated 10^7 times and values of $2\Delta\ln\mathcal{L} = 10.3$ or greater occurs with a frequency of 5.5×10^{-4}. This corresponds to a single sided fluctuation of a Gaussian distribution of 3.3σ, corresponding to evidence for the process $\Omega_b^- \to \Omega_c^0\,\pi^-$.

IV. PARTICLE PROPERTIES

The mass and lifetime of the b hadrons are measured by a fit with data binned in decay time, but not in mass [8]. The mass and signal yield in each ct bin are found by maximizing a likelihood given by

$$\mathcal{L} = \prod_j^{N_b} \prod_i^{N_j} \left[f_j \mathcal{P}_i^s + (1 - f_j)\mathcal{P}_{i,j}^b \right], \qquad (1)$$

where N_b is the number of ct bins chosen for the fit, N_j and f_j are the numbers of candidates and the signal fraction, respectively, for time bin j, and $\mathcal{P}_i^s$ and $\mathcal{P}_{i,j}^b$ are the mass probability density functions for the signal and background, respectively, for candidate i. The signal probability distribution is given by

$$\mathcal{P}_i^s = (1-\alpha)G(m_i, m_0, s_0\sigma_i^m) + \alpha G(m_i, m_0, s_1\sigma_i^m), \quad (2)$$

where G are Gaussians with average m_0; m_i and σ_i^m are the measured mass and uncertainty for candidate i; and α, s_0, and s_1 are parameters determined in the fit that describe, respectively, the relative contribution from each Gaussian and possible deviations between the calculated and true mass uncertainty. The background is modeled as

$$\mathcal{P}_{i,j}^b = \sum_{n=0}^{2} a_{n,j} P_n(m_i), \qquad (3)$$

where $P_n(m_i)$ are orthonormal polynomials of order n, which are normalized over the range of the fit, and $a_{n,j}$ are constants obtained in the fit. The background constants are obtained independently for each time range j. The overall normalization is assured by fixing $a_{0,j} = 1 - \sum_{n=1}^{2} a_{n,j}$.

The lifetime is determined by virtue of the fact that the fractional occupancy of each particular range of ct implies a specific lifetime for a particular measurement resolution. This is implemented in a two-step process,

which begins by maximizing the likelihood function in the mass distributions given in Eq. (1). In the second step, all parameters obtained in the mass fits are fixed and an additional lifetime term is added to the likelihood, rewriting it as

$$\mathcal{L} = \prod_j^{N_b} G(R_j, w_j(\tau,\sigma_\tau), \sigma_j^R) \prod_i^{N_j} \left[f_j \mathcal{P}_i^s + (1-f_j)\mathcal{P}_{i,j}^b \right], \tag{4}$$

where $R_j = f_j N_j / \sum_j f_j N_j$, σ_j^R is the uncertainty on R_j, and $w_j(\tau,\sigma_t)$ is the predicted fractional occupancy in each time range for lifetime τ measured with uncertainty σ_t. The predicted occupancy is found by integrating the decay-time distribution convoluted with the decay-time-measurement resolution, which is assumed to be Gaussian and is calculated analytically. Decay-time bins are chosen to have approximately equal occupancy for the initial lifetime chosen for the fit. The highest bin has no upper bound.

There are several advantages to this technique over the usual method of simultaneously fitting the signal and background lifetimes. The only distribution where signal and background components are fit together is the mass distribution in which these components are clearly discriminated given the differences in shape between the narrow signal distributions and the smooth, quasi-uniform background distributions. The number of parameters in the fit is limited, typically two for the mass, one for the lifetime, and two for each decay time bin to account for the yield and slope of the background. Finally, this method does not require a model of the effective decay-time distribution of the background.

Unless otherwise mentioned, all the implementations of the fit used in this analysis set the lowest limit of the lowest decay time bin to $ct = 100\,\mu$m, use an initial lifetime estimate of $ct = 450\,\mu$m, and utilize four decay-time bins ($N_b = 4$). Also, the decay time resolution is set so $\sigma_{ct} = 30\,\mu$m, which is typical of all candidates and is discussed further in Sec IV G. The lower limit of all mass fit ranges is chosen to be approximately one pion mass lower than the expected average mass of the reconstructed hadron in order to avoid backgrounds due to partially reconstructed states. Upper limits are chosen to obtain a reasonable estimate of the background.

A. The B meson reference signals

The $\mu^+\mu^-$ trigger data are well suited for use in particle property measurements. The trigger is insensitive to the decay time of any b hadron, so the corresponding samples are available for lifetime measurements without any trigger-induced bias. This data sample provides the B meson reference signals that are used to verify mass and lifetime measurement techniques used in this analysis. Mass measurements are obtained most directly from this fitting technique by using all candidates with $ct > 100\,\mu$m. The method reduces to the unbinned mass distribution fit that is traditionally used for mass measurements. Lifetime measurements are obtained by implementing the fit in several decay-time bins as described previously. As an example, the time-dependent mass distributions and decay-time distributions for the $B^0 \to J/\psi K_S^0$ reference signal are shown in Fig. 3. The results of the B^+ and B^0 measurements are listed in Table III and discussed in Sec. IV G.

B. Masses of the Ξ_c^0 and Ξ_c^+ baryons

The large samples of Ξ_c baryons in the full data set and the mass resolution available from the tracking system allow precise Ξ_c baryon mass measurements. The masses are obtained using the unbinned likelihood fit applied to all candidates with $ct > 100\,\mu$m. The $\Xi^-\pi^+$ and $\Xi^-\pi^+\pi^+$ mass distributions along with projections of the fits are shown in Fig. 4. Results from the mass fits are listed in Table IV.

C. Λ_b Measurements

The approach to fitting the mass and lifetime of the Λ_b is identical to that used for the meson reference signals. The mass distribution integrated in decay time and the projected fit are shown in Fig. 5. The decay-time-dependent mass distributions and decay-time distribution for the Λ_b candidates are shown in Fig. 6. Mass and lifetime results of the fits are listed in Table IV.

The effect of reflections from the $B^0 \to J/\psi\, K_S^0$, $K_S^0 \to \pi^+\pi^-$ decays is studied by recalculating the momenta of the $J/\psi\Lambda$ candidates reconstructed under the $B^0 \to J/\psi\, K_S^0$ hypothesis. We find 420 ± 29 candidates consistent with $B^0 \to J/\psi\, K_S^0$ decays within the $J/\psi\Lambda$ mass range used to fit the Λ_b. This B^0 background populates a portion of the $J/\psi\Lambda$ mass distribution that is systematically lower than the Λ_b mass. The shape of the B^0 background is parametrized and used as template for an additional background component in an alternative fit to the $J/\psi\Lambda$ mass distribution. The resulting Λ_b yield shifts by approximately 1% compared to the result obtained with the simple linear background, and is uniform over the time ranges. The total shift is approximately 20% of the statistical uncertainty in each time range, and fully correlated. We conclude that any effect due to the B^0 background is negligible with respect to other uncertainties. Any systematic shift in the lifetime measurement due to B^0 background treatment must be substantially less than 20% of the statistical uncertainty.

D. Ξ_b^- measurements

The approach to fitting the mass and lifetime of the Ξ_b^- is identical to that used for the meson reference signals.

TABLE III: B meson mass and $c\tau$ comparisons to known values [1]. Results from the entire data set (total) and the subset not included in the world averages (new) are listed. Only statistical uncertainties are listed.

Final state	Mass (MeV/c^2)		$c\tau(\mu$m)	
	Measured	Difference	Measured	Difference
$J/\psi\,K^+$ (total)	5278.75 ± 0.06	-0.5 ± 0.2	489.0 ± 2.1	-3.0 ± 3.0
$J/\psi\,K^+$ (new)	5278.74 ± 0.08	-0.5 ± 0.2	491.9 ± 3.0	-0.1 ± 3.8
$J/\psi\,K^{0*}$ (total)	5279.01 ± 0.11	-0.5 ± 0.2	458.6 ± 3.3	3.2 ± 3.9
$J/\psi\,K^{0*}$ (new)	5278.95 ± 0.17	-0.6 ± 0.2	458.4 ± 4.7	3.0 ± 5.1
$J/\psi\,K^0_s$ (total)	5280.03 ± 0.12	0.4 ± 0.2	458.6 ± 4.2	3.2 ± 4.6
$J/\psi\,K^0_s$ (new)	5280.09 ± 0.18	0.5 ± 0.2	461.0 ± 5.9	5.6 ± 6.1

TABLE IV: Baryon mass and lifetime results. Only statistical uncertainties are listed .

Final state	Mass (MeV/c^2)	$c\tau(\mu$m)	Yield
$\Xi_c^0(\Xi^-\,\pi^+)$	2470.85 ± 0.24	-	3582 ± 82
$\Xi_c^+(\Xi^-\,\pi^+\,\pi^+)$	2468.00 ± 0.18	-	5714 ± 108
$\Lambda_b(J/\psi\,\Lambda)$	5620.15 ± 0.31	468.4 ± 10.5	2920 ± 120
$\Xi_b^-(J/\psi\,\Xi^-)$	5793.2 ± 1.9	396 ± 43	112 ± 19
$\Xi_b^-(\Xi_c^0\,\pi^-)$	5794.8 ± 5.0	-	33 ± 6
$\Xi_b^0(\Xi_c^+\,\pi^-)$	5788.7 ± 4.3	-	62 ± 9
$\Omega_b^-(J/\psi\,\Omega^-)$	6050.0 ± 4.1	497^{+159}_{-119}	22 ± 6
$\Omega_b^-(\Omega_c^0\,\pi^-)$	6029 ± 11	-	$5.5\pm^{+2.5}_{-2.4}$

The mass distributions for the $J/\psi\,\Xi^-$ and $\Xi_c^0\,\pi^-$ combinations integrated in decay time and the projected fits are shown in Fig. 7. The time-dependent mass distributions and decay-time distribution for the $\Xi_b^- \to J/\psi\,\Xi^-$ channel are shown in Fig. 8. Mass and lifetime results of the fits are listed in Table IV.

E. Ξ_b^0 measurements

The process $\Xi_b^0 \to J/\psi\,\Xi^0$ is expected to occur, in analogy to $\Xi_b^- \to J/\psi\,\Xi^-$. However, this process requires the accurate reconstruction of a low-momentum π^0, so it is outside the sensitivity of this experiment. Consequently, we are limited to a Ξ_b^0 mass measurement in the $\Xi_b^0 \to \Xi_c^+\,\pi^-$ channel. The $\Xi_c^+\,\pi^-$ mass distribution and the projection of the fit overlaid on the data are shown in Fig. 9, and the fit result is listed in Table IV.

F. Ω_b^- measurements

The approach of fitting the mass and lifetime of the Ω_b^- is identical to that used for the meson reference signals, with the exception that only three decay-time ranges are used in the lifetime calculation due to the small sample of candidates. The mass distributions for the $J/\psi\,\Omega^-$ and $\Omega_c^0\,\pi^-$ combinations integrated in decay time and the projected fits are shown in Fig. 10. The time-dependent mass distributions and decay-time distribution for the $\Omega_b^- \to J/\psi\,\Omega^-$ channel are shown in Fig. 11. The mass resolution terms s_0 are fixed to the values obtained in the analogous channels used in the Ξ_b^- fits. The results of the mass and lifetime fits are listed in Table IV.

G. Systematic uncertainties

The systematic uncertainties on the mass measurements reported here are similar to those obtained for other b hadrons in previous CDF II analyses. The mass scale uncertainty is taken from earlier work [23]. Here, the J/ψ, $\psi(2S)$ and Υ decays, reconstructed in dimuon final states, were used to set the mass scale. The differences of the measured masses from the true masses are parametrized as functions of the total kinetic energy in these decays and are then used to obtain the mass scale uncertainties listed in Table V. The effect of the mass-resolution model on the mass-uncertainty scale is tested in several variations of the fits on the B meson and Ξ_c baryon signals. These variations indicate that the choice of resolution model can affect the resulting mass measurement by 0.05 – 0.1 MeV/c^2. The effect of the tracking-system material on the mass scale is tested by examining the mass of the B^0 reconstructed in the $J/\psi\,K^0_S$ channel as a function of the K^0_S decay point. A systematic shift of 1.1 ± 0.5 MeV/c^2 is found for combinations where the K^0_S decay point is outside the silicon system. In order to determine the sensitivity of b-baryon reconstruction to the tracking-system material, we determine the fraction of b-baryon candidates whose Λ, Ξ^-, or Ω^- decay outside the silicon system by using the data for the Ξ_c and Λ_b baryons and simulation for the Ξ_b and Ω_b^- baryons. This fraction of the shift observed in B^0 decays is taken for a systematic uncertainty on the mass due to material description of the detector. Masses of the p, π^-, K^-, and Λ are sufficiently well determined that their contribution to the systematic uncertainty is insignificant. These effects are listed in Table V, where they are combined in

quadrature to obtain the total systematic uncertainties.

The B mesons reconstructed in the J/ψ sample serve as a precision reference sample to support the evaluation of the systematic uncertainties. The mass and lifetime results obtained for the B^+ and B^0 are listed in Table III. Comparisons between the measurements and the known values [1] are listed. The known values contain contributions from a subset of the CDF Run II data [23, 24]. Consequently, values are given for the full data set and the data taken since the previous measurement [8]. We find the more recent data to be completely consistent with our earlier measurements, indicating that no significant degradation of the tracking resolution occurred. A comparison of the results in reference signals with the known values demonstrates that the mass measurements are well understood.

The masses of the Ξ_b^- and Ω_b^- baryons are each measured in two different final states. The mass results are combined to provide a single measurement following Ref. [27]. These combined results, and the mass results for the other baryons, are listed in Table VI. The momentum scale uncertainty cancels in measurements of the mass differences between the Ξ_c^0 and Ξ_c^+, and the Ξ_b^- and Ξ_b^0 baryons. The estimates for these isospin splittings are also listed in Table VI.

The lifetime fit is repeated on the reference signals to determine the sensitivity of the technique to the input parameters chosen for the fit. The decay-time uncertainty σ_{ct} is shown in Fig. 12 for the $B^0 \to J/\psi\, K_S^0$ sample, where the background contribution is removed by subtracting mass sideband uncertainties. If this uncertainty is varied between 15 and 45 μm, the results of the lifetime fit are found to have a relative variation of less than 10^{-3}. Variations in the number of decay-time bins have similar impact.

Systematic uncertainties on the lifetime measurements of the b baryons are identical to those of the B mesons. The B meson reference signals all have lifetime results that are within 1% of their known values, as is shown in Table III. If we use only the recent data for the $B^0 \to J/\psi\, K_S^0$ process, we find complete consistency with the known lifetime within $\pm 6\,\mu$m, or 1.3%. This is taken as the systematic uncertainty for all b-baryon lifetime measurements.

V. FINAL RESULTS

Final results for the properties of the b baryons are listed in Tables VI and VII. The measurements of the masses of the Ξ_c baryons are competitive with the world averages, and consistent with them [1]. The isospin splitting of the states is also comparable to the world average. These measurements serve to improve our overall knowledge of heavy baryon dynamics. Theoretical calculations of the Ξ_c baryon masses are not as precise as the current measurements, so these results serve to constrain the models considered for heavy baryon mass predictions [2, 3]. As with the charmed baryons, the Λ_b mass is now known with high precision. All other b baryons are currently only seen in small samples, so the measurements are limited by the sample size. The mass obtained for the Ξ_b^0 confirms our earlier observation [9] and provides a small improvement to our unique measurement of the isospin splitting in the Ξ_b system, which is consistent with the prediction of Ref. [3]. The present measurement of the mass of the Ω_b^- provides further support to our first result [8] and is inconsistent with the measurement associated with the first observation of this particle [7].

The precision of the measurement of the lifetime of the Λ_b baryon is comparable to that of the B^0 meson. By combining the two reference measurements of the B^0 and retaining the full systematic uncertainty found in Sect. IV G, we obtain $\tau(\Lambda_b)/\tau(B^0) = 1.021 \pm 0.024(\text{stat}) \pm 0.013(\text{syst})$, which is more consistent with the predicted values [25, 26] than earlier measurements. The lifetime measurements of the Ξ_b^- and Ω_b^- baryons are unique and limited by the size of the samples. The values obtained appear to be typical of other b hadrons.

VI. CONCLUSIONS

In conclusion, the CDF Run II data set is analyzed to identify the largest possible low-background sample of Ξ_c and b-baryon ground states. The mass and lifetime properties of these particles are measured, and the results compared to precisely measured quantities for B mesons obtained in similar final states. The mass and isospin splitting of the Ξ_c system are measured with precisions that are comparable to the world averages. The first evidence for the process $\Omega_b^- \to \Omega_c^0\,\pi^-$ is shown. The masses and lifetimes of the Λ_b, Ξ_b^- and Ω_b^- baryons are measured and are found consistent with LHCb determinations [10, 15, 28]. The isospin splitting of the Ξ_b system is unique to this experiment and is updated with the final data set. These results supersede previous measurements, which were obtained using a subset of these data [8, 9].

We thank the Fermilab staff and the technical staffs of the participating institutions for their vital contributions. This work was supported by the U.S. Department of Energy and National Science Foundation; the Italian Istituto Nazionale di Fisica Nucleare; the Ministry of Education, Culture, Sports, Science and Technology of Japan; the Natural Sciences and Engineering Research Council of Canada; the National Science Council of the Republic of China; the Swiss National Science Foundation; the A.P. Sloan Foundation; the Bundesministerium für Bildung und Forschung, Germany; the Korean World Class University Program, the National Research Foundation of Korea; the Science and Technology Facilities Council and the Royal Society, United Kingdom; the Russian Foundation for Basic Research; the Ministerio de Ciencia e Innovación, and Programa Consolider-Ingenio

TABLE V: Contributions to the systematic uncertainty on the mass measurements.

Source	Uncertainty (MeV/c^2)									
	Ξ_c^0	Ξ_c^+	B^0		Λ_b	Ξ_b^-		Ξ_b^0	Ω_b^-	
			$J/\psi K^{0*}$	$J/\psi K_S^0$		$J/\psi\Xi^-$	$\Xi_c^0\pi^-$		$J/\psi\Omega^-$	$\Omega_c^0\pi^-$
Mom. scale	0.35	0.35	0.42	0.45	0.40	0.40	0.50	0.40	0.40	0.55
Reso. model	0.05	0.05	0.1	0.1	0.1	0.1	0.1	0.1	0.1	0.1
Material	0.38	0.38	0.0	0.25	0.21	0.47	1.16	1.15	0.38	0.94
Total	0.55	0.51	0.43	0.53	0.47	0.6	1.4	1.4	0.6	1.2

TABLE VI: Ξ_c and b-baryon mass results. The first uncertainty listed is statistical and the second is systematic.

Baryon	Mass (MeV/c^2)
Ξ_c^0	$2470.85 \pm 0.24 \pm 0.55$
Ξ_c^+	$2468.00 \pm 0.18 \pm 0.51$
Λ_b	$5620.15 \pm 0.31 \pm 0.47$
Ξ_b^-	$5793.4 \pm 1.8 \pm 0.7$
Ξ_b^0	$5788.7 \pm 4.3 \pm 1.4$
Ω_b^-	$6047.5 \pm 3.8 \pm 0.6$
$M(\Xi_c^0) - M(\Xi_c^+)$	$2.85 \pm 0.30 \pm 0.04$
$M(\Xi_b^-) - M(\Xi_b^0)$	$4.7 \pm 4.7 \pm 0.7$

TABLE VII: b-baryon lifetime results. The first uncertainty listed is statistical and the second is systematic.

Baryon	lifetime (ps)
Λ_b	$1.565 \pm 0.035 \pm 0.020$
Ξ_b^-	$1.36 \pm 0.15 \pm 0.02$
Ω_b^-	$1.66^{+0.53}_{-0.40} \pm 0.02$

2010, Spain; the Slovak R&D Agency; the Academy of Finland; the Australian Research Council (ARC); and the EU community Marie Curie Fellowship Contract No. 302103.

[1] J. Beringer *et al.* (Particle Data Group), Phys. Rev. D **86**, 010001 (2012) and 2013 update for the 2014 edition.

[2] E. Jenkins, Phys. Rev. D **77**, 034012 (2008); R. Lewis and R. M. Woloshyn, *ibid.* **79**, 014502 (2009); D. Ebert, R. N. Faustov and V. O. Galkin, *ibid.* **72**, 034026 (2005); A. Valcarce, H. Garcilazo, and J. Vijande, Eur. Phys. J. A **37**, 217 (2008).

[3] M. Karliner, B. Keren-Zur, H. J. Lipkin, and J. L. Rosner, Ann. Phys. (N.Y.) **324**, 2 (2009).

[4] V. M. Abazov *et al.* (D0 Collaboration), Phys. Rev. Lett. **99**, 052001 (2007).

[5] T. Aaltonen *et al.* (CDF Collaboration), Phys. Rev. Lett. **99**, 052002 (2007).

[6] T. Aaltonen *et al.* (CDF Collaboration), Phys. Rev. D **85**, 092011 (2012).

[7] V. M. Abazov *et. al.* (D0 Collaboration), Phys. Rev. Lett. **101**, 232002 (2008).

[8] T. Aaltonen *et al.* (CDF Collaboration), Phys. Rev. D **80**, 072003 (2009).

[9] T. Aaltonen *et al.* (CDF Collaboration), Phys. Rev. Lett. **107**, 102001 (2011).

[10] R. Aaij *et al.* (LHCb Collaboration), Phys. Rev. Lett. **110**, 182001 (2013).

[11] S. Chatrchyan *et al.* (CMS Collaboration), Phys. Rev. Lett. **108**, 252002 (2012).

[12] R. Aaij *et al.* (LHCb Collaboration), Phys. Rev. Lett. **109**, 172003 (2012).

[13] T. Aaltonen *et al.* (CDF Collaboration), Phys. Rev. D. **88**, 071101 (2013).

[14] F. Gabbiani, A. Onishchenko, and A. Petrov, Phys. Rev. D **70**, 094031 (2004).

[15] R. Aaij *et al.* (LHCb Collaboration), Phys. Rev. Lett. **111**, 102003 (2013).

[16] D. Acosta *et al.* (CDF Collaboration), Phys. Rev. D **71**, 032001 (2005); T. Affolder *et al.*, Nucl. Instrum. Methods, Sec. A **526**, 249 (2004).

[17] T. Aaltonen *et al.*, Nucl. Instrum. Methods, Sec. A **729**, 153 (2013).

[18] T. Affolder *et al.*, Nucl. Instrum. Methods, Sec. A **526**, 249 (2004).
[19] G.Ascoli *et al.*, Nucl. Instrum. Methods, Sec. A **268**, 33 (1988).
[20] L. Ristori and G. Punzi, Ann. Rev. Nucl. Sci. **60**, 595 (2010); W. Ashmanskas *et al.*, Nucl. Instrum. Methods, Sec. A **518**, 534 (2004).
[21] D.J. Lange, Nucl. Instrum. Methods, Sec. A **462**, 152 (2001).
[22] R. Brun, R. Hagelberg, M. Hansroul, and J.C. Lassalle, CERN Reports No. CERN-DD-78-2-REV and No. CERN-DD-78-2.
[23] D. Acosta *et al.* (CDF Collaboration), Phys. Rev. Lett. **96**, 202001 (2006).
[24] T. Aaltonen *et al.* (CDF Collaboration), Phys. Rev. Lett. **106**, 121804 (2011).
[25] M. Neubert and C.T. Sachrajda, Nucl. Phys. B **483**, 339 (1997).
[26] J. Rosner, Phys. Lett. B **379**, 267 (1996).
[27] L. Lyons, D. Gibaut, and P. Clifford, Nucl. Instrum. Methods A **270**, 110 (1988).
[28] R. Aaij *et al.* (LHCb Collaboration), Phys. Rev. D **89**, 032001 (2014).

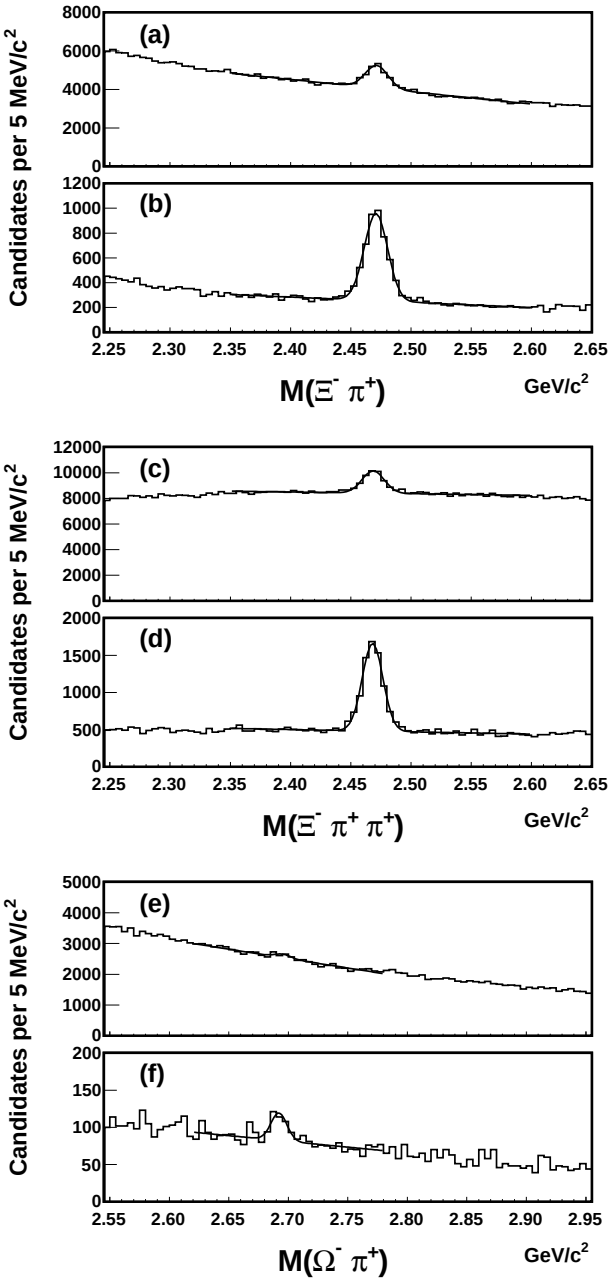

FIG. 1: Distribution of $\Xi^-\,\pi^+$ mass for (a) all candidates and (b) the subset where the Ξ^- is tracked in the silicon detector and the impact parameter with respect to the beamline is less than 100 μm. Panels (c,d) and (e,f) show similar distributions for $\Xi^-\,\pi^+\,\pi^+$ and $\Omega^-\,\pi^+$ candidates, respectively.

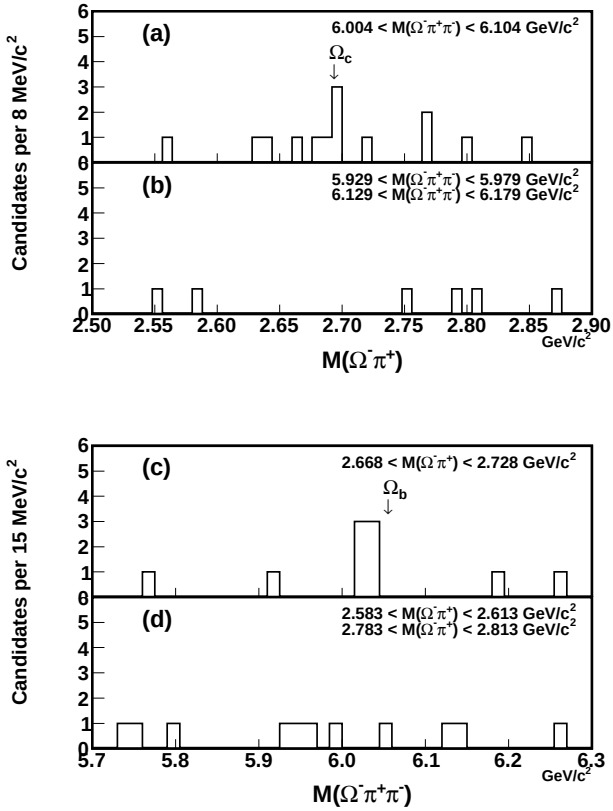

FIG. 2: Distribution of $\Omega^-\,\pi^+$ (a,b) and $\Omega^-\,\pi^+\,\pi^-$ (c,d) mass for candidates obtained from the Ω_b^- selection. Panel (a) shows the $\Omega^-\,\pi^+$ mass for candidates consistent with the $\Omega_b^- \to \Omega^-\pi^+\,\pi^-$ signal region; panel (b) shows the $\Omega^-\,\pi^+$ mass for candidates restricted to the Ω_b^- mass sidebands. Panel (c) shows the $\Omega^-\,\pi^+\,\pi^-$ mass for candidates consistent with the $\Omega_c^0 \to \Omega^-\,\pi^+$ signal region; panel (d) shows the $\Omega^-\,\pi^+\,\pi^-$ mass for candidates restricted to the Ω_c^0 mass sidebands.

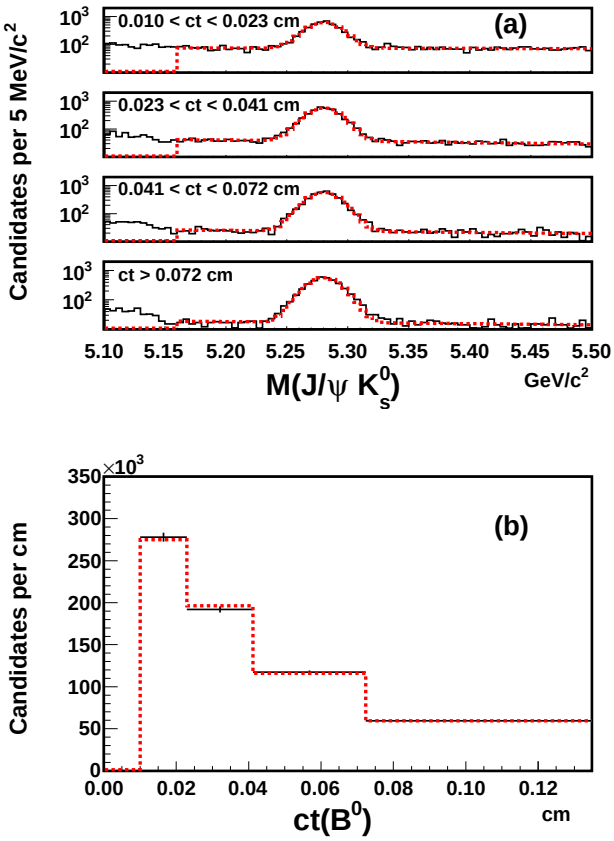

FIG. 3: Distributions of (a) $J/\psi\, K^0_S$ mass and (b) ct for B^0 reconstructed in the $B^0 \to J/\psi\, K^0_S$ decay. The mass and lifetime fits are overlaid in dashed red. For display purposes, the upper limit of the ct distribution is chosen to be 0.135 cm so that the displayed distribution contains 95% of the candidates, based on the initial lifetime estimate.

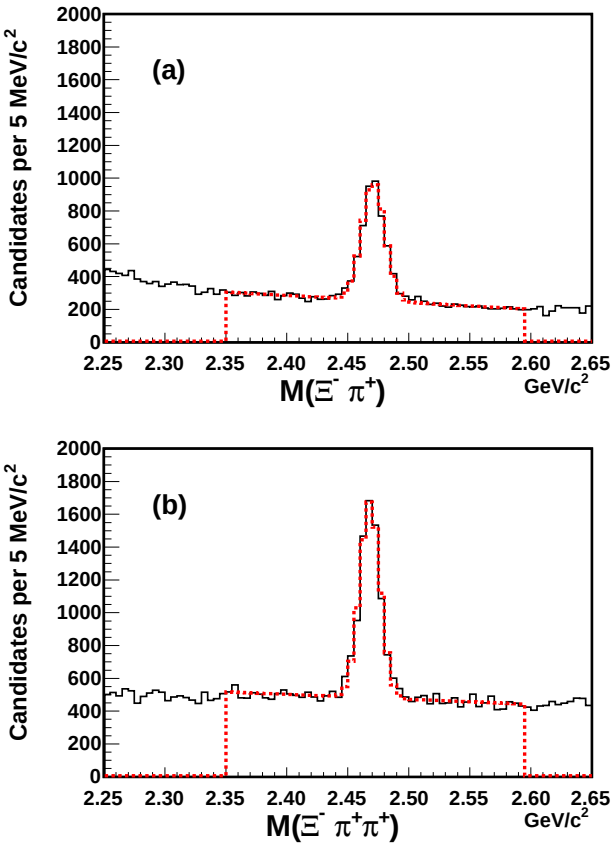

FIG. 4: Distribution of (a) $\Xi^-\,\pi^+$ and (b) $\Xi^-\,\pi^+\,\pi^+$ mass used for the Ξ_c mass measurements. The fits are overlaid on the data in dashed red.

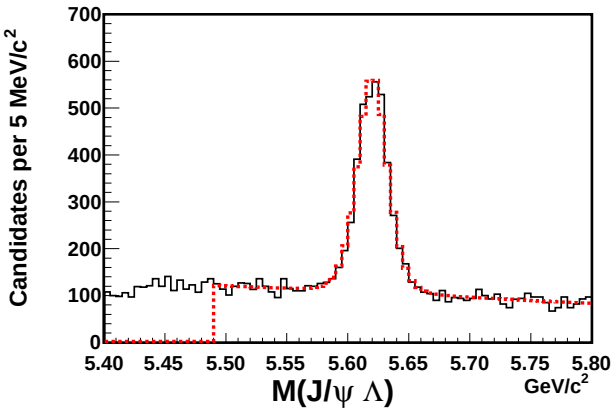

FIG. 5: Distribution of $J/\psi\,\Lambda$ mass used for the Λ_b mass measurement. The fit is overlaid on the data in dashed red.

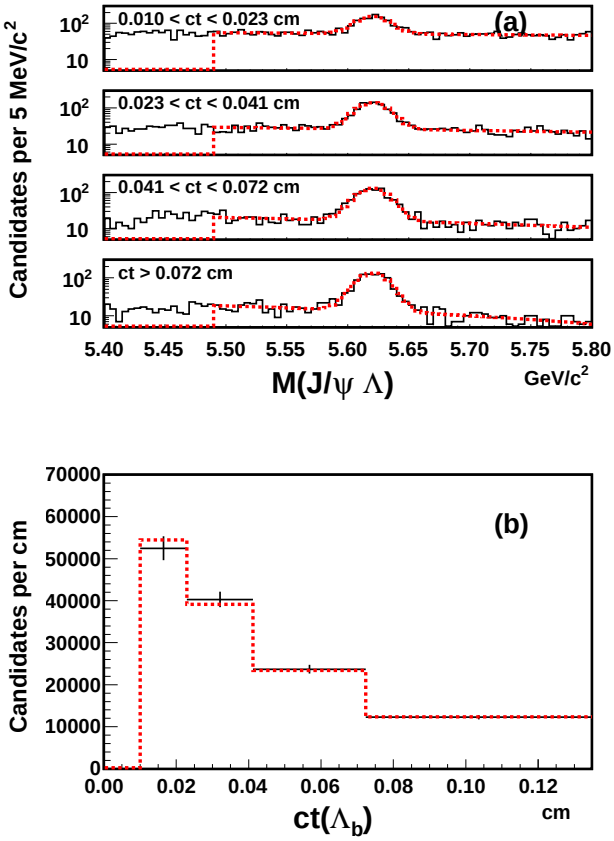

FIG. 6: Distribution of (a) $J/\psi\,\Lambda$ mass divided into four independent decay-time ranges and (b) ct of Λ_b candidates used to calculate the lifetime. The fits are overlaid on the data in dashed red.

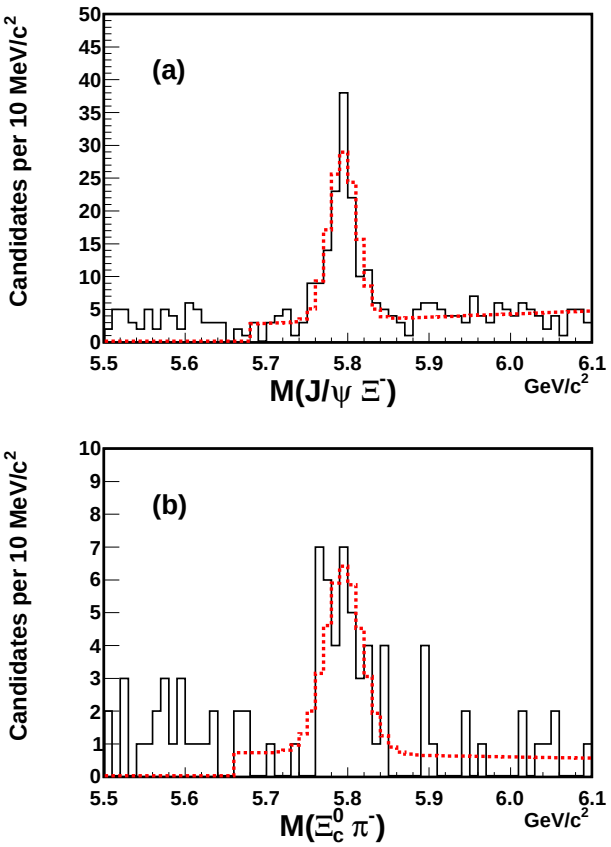

FIG. 7: Distribution of (a) the $J/\psi\,\Xi^-$ and (b) $\Xi_c^0\,\pi^-$ mass used for the Ξ_b^- mass measurements. The fits are overlaid on the data in dashed red.

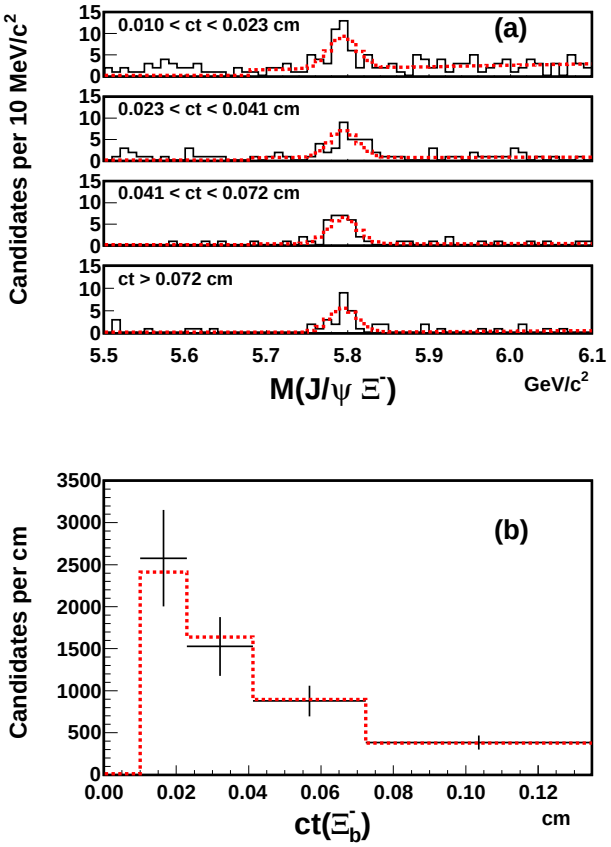

FIG. 8: Distribution of (a) $J/\psi\,\Xi^-$ mass divided into four independent decay-time ranges and (b) ct of Ξ_b^- candidates used to calculate the lifetime. The fits are overlaid on the data in dashed red.

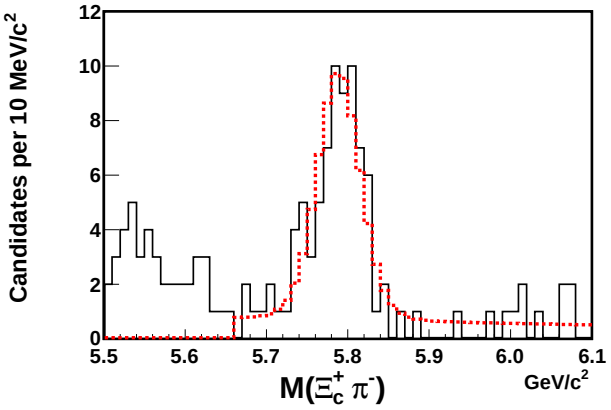

FIG. 9: Distribution of $\Xi_c^+\,\pi^-$ mass used for the Ξ_b^0 mass measurement. The fit is overlaid on the data in dashed red.

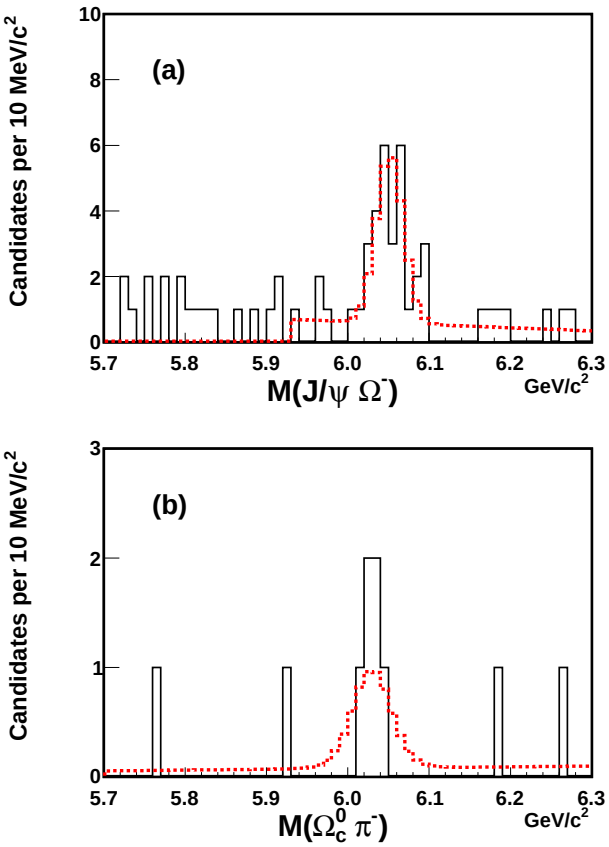

FIG. 10: Distribution of (a) $J/\psi\,\Omega^-$ and (b) $\Omega_c^0\,\pi^-$ mass used for the Ω_b^- mass measurement. The fits are overlaid on the data in dashed red.

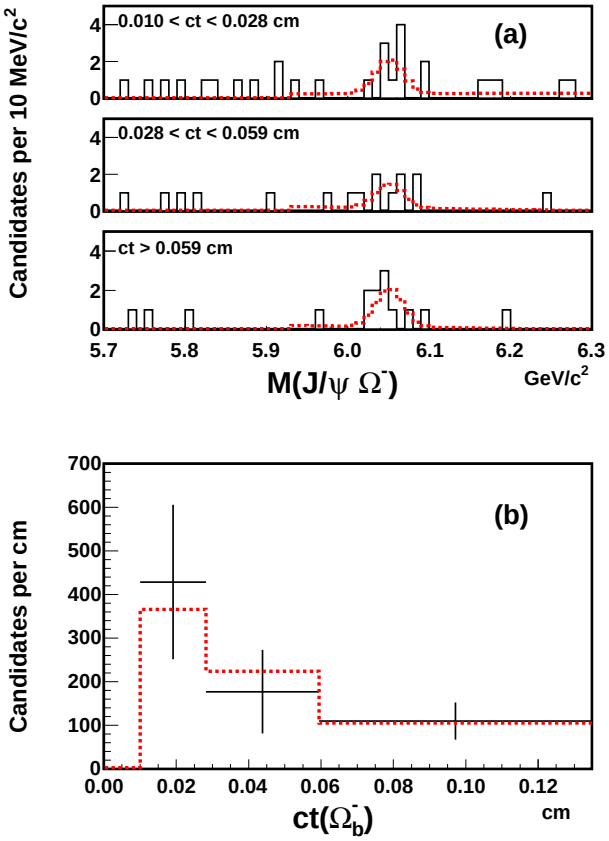

FIG. 11: Distribution of (a) $J/\psi\,\Omega^-$ mass divided into three independent decay-time ranges and (b) ct of Ω_b^- candidates used to calculate the lifetime. The fits are overlaid on the data in dashed red.

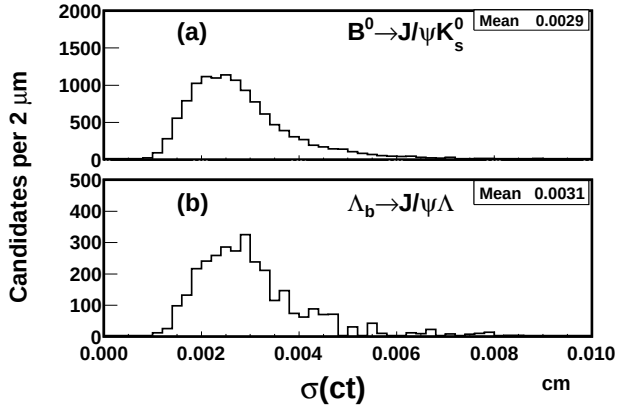

FIG. 12: Distribution of σ_{ct} for (a) $B^0 \to J/\psi\,K_S^0$ candidates and (b) $\Lambda_b \to J/\psi\,\Lambda$ candidates.